Enhanced ultrafast infrared spectroscopy using coupled nanoantenna arrays

F. KUSA,[1,2] I. MORICHIKA,[1] A. TAKEGAMI,[1,2] AND S. ASHIHARA[1,*]

[1]*Institute of Industrial Science, The University of Tokyo, 4-6-1, Komaba, Meguro-ku, Tokyo, 153-8505, Japan*
[2]*Department of Applied Physics, Tokyo Univ. of Agriculture and Technology, 2-24-16, Nakacho, Koganei, Tokyo, 184-8588, Japan*
[*]*ashihara@iis.u-tokyo.ac.jp*

Abstract: Surface-enhanced nonlinear vibrational spectroscopy using periodic gold nanoantenna arrays is demonstrated. The dipolar coupling among arrayed nanoantennas is shown to have striking impact on near-field enhancements of femtosecond pulsed-fields and on nonlinear signal enhancements. The condition near the collective-resonance achieves averaged signal enhancement of 850 times and local signal enhancement of 1.8×10^6 times, substantially reducing the required pump energy from micro-joule to nano-joule level. The scheme is useful for characterizing structure and dynamics of minute-volume molecular samples, monolayers, and interfaces, as well as paves the way to nonlinear vibrational spectroscopy with compact light sources of oscillator-level.

© 2017 Optical Society of America

OCIS codes: (320.7150) Ultrafast spectroscopy; (300.6340) Spectroscopy, infrared; (240.6680) Surface plasmons.

References and links

1. P. Hamm and M. Zanni, *Concepts and methods of 2D infrared spectroscopy* (Cambridge University Press, 2011).
2. E. T. J. Nibbering and T. Elsaesser, "Ultrafast vibrational dynamics of hydrogen bonds in the condensed phase," Chem. Rev. **104**(4), 1887–1914 (2004).
3. A. Hartstein, J. R. Kirtley, and J. C. Tsang, "Enhancement of the infrared-absorption from molecular monolayers with thin metal overlayers," Phys. Rev. Lett. **45**(3), 201–204 (1980).
4. M. Osawa and M. Ikeda, "Surface-enhanced infrared-absorption of para-nitrobenzoic acid deposited on silver island films - contributions of electromagnetic and chemical mechanisms," J. Phys. Chem. **95**(24), 9914–9919 (1991).
5. F. Neubrech, A. Pucci, T. W. Cornelius, S. Karim, A. García-Etxarri, and J. Aizpurua, "Resonant plasmonic and vibrational coupling in a tailored nanoantenna for infrared detection," Phys. Rev. Lett. **101**(15), 157403 (2008).
6. R. Adato, A. A. Yanik, J. J. Amsden, D. L. Kaplan, F. G. Omenetto, M. K. Hong, S. Erramilli, and H. Altug, "Ultra-sensitive vibrational spectroscopy of protein monolayers with plasmonic nanoantenna arrays," Proc. Natl. Acad. Sci. U.S.A. **106**(46), 19227–19232 (2009).
7. P. M. Donaldson and P. Hamm, "Gold nanoparticle capping layers: structure, dynamics, and surface enhancement measured using 2D-IR spectroscopy," Angew. Chem. Int. Ed. Engl. **52**(2), 634–638 (2013).
8. F. Kusa and S. Ashihara, "Spectral response of localized surface plasmon in resonance with mid-infrared light," J. Appl. Phys. **116**(15), 153103 (2014).
9. F. Kusa, K. E. Echternkamp, G. Herink, C. Ropers, and S. Ashihara, "Optical field emission from resonant gold nanorods driven by femtosecond mid-infrared pulses," AIP Adv. **5**(7), 077138 (2015).
10. O. Selig, R. Siffels, and Y. L. A. Rezus, "Ultrasensitive ultrafast vibrational spectroscopy employing the near field of gold nanoantennas," Phys. Rev. Lett. **114**(23), 233004 (2015).
11. B. Auguié and W. L. Barnes, "Collective resonances in gold nanoparticle arrays," Phys. Rev. Lett. **101**(14), 143902 (2008).
12. R. Adato, A. A. Yanik, C.-H. Wu, G. Shvets, and H. Altug, "Radiative engineering of plasmon lifetimes in embedded nanoantenna arrays," Opt. Express **18**(5), 4526–4537 (2010).
13. D. Weber, P. Albella, P. Alonso-González, F. Neubrech, H. Gui, T. Nagao, R. Hillenbrand, J. Aizpurua, and A. Pucci, "Longitudinal and transverse coupling in infrared gold nanoantenna arrays: long range versus short range interaction regimes," Opt. Express **19**(16), 15047–15061 (2011).
14. V. Liberman, R. Adato, T. H. Jeys, B. G. Saar, S. Erramilli, and H. Altug, "Rational design and optimization of plasmonic nanoarrays for surface enhanced infrared spectroscopy," Opt. Express **20**(11), 11953–11967 (2012).
15. S. Bagheri, K. Weber, T. Gissibl, T. Weiss, F. Neubrech, and H. Giessen, "Fabrication of square-centimeter plasmonic nanoantenna arrays by femtosecond direct laser writing lithography: effects of collective excitations on SEIRA enhancement," ACS Photonics **2**(6), 779–786 (2015).

16. Y. S. Joe, A. M. Satanin, and C. S. Kim, "Classical analogy of Fano resonances," Phys. Scr. **74**(2), 259–266 (2006).
17. Y. L. Rezus and O. Selig, "Impact of local-field effects on the plasmonic enhancement of vibrational signals by infrared nanoantennas," Opt. Express **24**(11), 12202–12227 (2016).
18. B. J. Messinger, K. U. Vonraben, R. K. Chang, and P. W. Barber, "Local fields at at the surface of noble-metal microspheres," Phys. Rev. B **24**(2), 649–657 (1981).
19. M. Banno, S. Sato, K. Iwata, and H. Hamaguchi, "Solvent-dependent intra- and intermolecular vibrational energy transfer of W(CO)$_6$ probed with sub-picosecond time-resolved infrared spectroscopy," Chem. Phys. Lett. **412**(4–6), 464–469 (2005).
20. S. Ashihara, K. Shibuya, and S. Fujioka, "Temperature dependence of vibrational relaxation of the OH bending excitation in liquid H$_2$O," Chem. Phys. Lett. **502**(1–3), 57–62 (2011).
21. X. L. Wang, Y. Guillet, P. R. Selvakannan, H. Remita, and B. Palpant, "Broadband spectral signature of the ultrafast transient optical response of gold nanorods," J. Phys. Chem. C **119**(13), 7416–7427 (2015).
22. F. Neubrech, S. Beck, T. Glaser, M. Hentschel, H. Giessen, and A. Pucci, "Spatial extent of plasmonic enhancement of vibrational signals in the infrared," ACS Nano **8**(6), 6250–6258 (2014).
23 I. Morichika, F. Kusa, A. Takegami, A. Sakurai, and S. Ashihara, "Antenna-enhanced nonlinear infrared spectroscopy in reflection geometry," J. Phys. Chem. C (to be published) (2017).

1. Introduction

Nonlinear vibrational spectroscopy employing mid-infrared (MIR) ultrashort pulses provides powerful tools in elucidating molecular structure and dynamics [1,2]. Pump-probe absorption spectroscopy and two-dimensional correlation spectroscopy resolve vibrational relaxation dynamics, structural dynamics, mode couplings, conformations, environmental fluctuations, etc. The applications are, however, somewhat limited because infrared (IR) transition dipole moments of vibrational modes are generally small. Although the absorption cross-sections of IR active modes are typically ~10 orders of magnitude larger than the corresponding non-resonant Raman cross-sections (~6 orders of magnitude larger than the corresponding resonant Raman cross-sections), they are ~3 orders of magnitude smaller than UV-Vis absorption/fluorescence cross-sections. Therefore the measurements require MIR pulses of micro-joule level, typically generated from the complex laser system consisting of the femtosecond regenerative amplifier and the subsequent frequency converters. The fact that the required light-source is bulky, complex, and expensive restricts the wide-spread use of the nonlinear vibrational spectroscopy. Furthermore, even if the MIR pulses of micro-joule level are exploited, nonlinear signals can be observed only for a limited number of vibrational modes whose transition dipole moments are relatively large (e.g., CO, NH, OH stretching vibrations). These issues would be solved if the interactions between MIR light and molecular vibrations are substantially enhanced.

It is known that linear vibrational signals of molecules adsorbed on rough metal surfaces are amplified in the IR absorption spectroscopy (surface-enhanced infrared absorption: SEIRA) [3,4]. The mechanisms of signal enhancements were attributed to near-field enhancements and chemical effects [4], the former of which originated from off-resonant plasmonic responses of metal nanoparticles. In the last decade, metal nanoantennas resonating at MIR frequencies were applied to linear vibrational spectroscopy [5,6].

Plasmonic near-field enhancements promise to enhance nonlinear vibrational signals as well. Rather, the enhancements would be more substantial because nonlinear signals increase super-linearly with field-amplitudes. So far, nonlinear IR spectroscopy on capping layers of gold nanoparticles has been demonstrated, where nonlinear signals were enhanced by off-resonant plasmonic responses of nanoparticles [7]. Near-field enhancements of MIR femtosecond pulses by resonant meal nanoantennas have been studied [8] and successfully applied to nonlinear photoemissions [9]. Recently, nonlinear IR spectroscopy has been demonstrated by employing resonant gold nanoantennas by Selig et al. [10]. The authors performed pump-probe and two-dimensional spectroscopies on 5 nm layers of polymethylmetacrylate (PMMA) with randomly-arranged nanoantennas and observed the nonlinear signal enhancement factors of more than 4 orders of magnitude. Engineerable

properties of metal nanoantenna arrays, however, has not been explored for benefitting nonlinear vibrational spectroscopy.

In this paper, we demonstrate that the dipolar coupling among nanoantennas has striking impact on near-field enhancements and nonlinear vibrational signal enhancements. We employ periodic arrangement to control the radiative damping rate and the resultant near-field enhancements [6,11–15]. Compared with random arrangement, where the dipolar coupling among nanoantennas is inhomogeneous and cancelled out as an ensemble average [6], the dipolar coupling is homogeneous over whole array area in periodic arrangement. Therefore it is possible to engineer the radiative damping for higher field enhancements and the resultant signal enhancements. The condition near the collective-resonance achieves averaged signal enhancement of 850 times and local signal enhancement of 1.8×10^6 times, reducing required pump energy from micro-joule to nano-joule level. Such substantial signal enhancement, together with surface sensitivity, is useful for characterizing structure and dynamics of minute-volume molecular samples, monolayers, and interfaces, and for detecting vibrational modes with smaller transition moments. It also paves the way to nonlinear vibrational spectroscopy with compact light sources of oscillator-level.

2. Near-field enhancements of femtosecond pulses

2.1 Near-field enhancements by coupled nanoantenna arrays

Rod-shaped metal nanoantennas (or nanorods) exhibit near-field enhancements in the vicinity of nanorod-ends, owing to half-wave dipole antenna resonance and geometrical effects (or the lightning rod effect). Resonance frequency is determined by size and shape of a nanorod and by surrounding material. In particular, metal nanorods of few-micron lengths exhibit their resonances in the MIR spectral range [5,6,8].

The radiative damping rate or the resonant linewidth can be engineered by controlling the dipolar coupling among neighboring nanorods [6,11–15]. The simplest example is the 1D periodic array, where an identical nanorod is arranged with a constant pitch in the direction perpendicular to the nanorod. For a 1D periodic array illuminated by a monochromatic wave under the normal incidence, constructive interference happens between incident field and scattered field, when the array pitch equals multiples of the effective wavelength. Here the nanorods are excited not only resonantly but also collectively, and the radiative damping is substantially modified. In view of applying such linewidth engineering to enhanced ultrafast spectroscopy, we investigate temporal/spectral properties of the near-field enhancements.

Electromagnetic field distribution around gold nanorod arrays on a CaF_2 substrate (refractive index of ~1.4 at a wavelength of 5 μm), upon polychromatic light illumination, is numerically simulated by the finite-difference time-domain (FDTD) method. Here each nanorod is modeled using a rectangular cross-section and two half-cylinders at both ends. The spectral transfer function $H(\omega)$ at each frequency ω is derived as the local-field at a position in the vicinity of the nanorod end (5 nm away from the nanorod end and at the center in directions of width and height of the nanorod), $E_{lo}(\omega)$, divided by the incident light-field $E_{in}(\omega)$: $H(\omega) = E_{lo}(\omega)/E_{in}(\omega)$ [8]. Figure 1(a) shows the calculated field enhancement factor $|H(\omega)|$ for nanorod arrays with rectangular lattice arrangements. Here dimensions of each nanorod (length: 1200 nm, width: 200 nm, height: 30 nm) and the arrangement period along longer-axis (d_x ~2.0 μm) are fixed, whereas the arrangement period along shorter-axis is varied. In these arrangements, near-field coupling among neighboring nanorods has negligible effect but the radiative (or dipolar) coupling does modify the plasmonic responses. The field enhancement spectrum for the isolated nanorod and those for the arrays of d_y = 1.0, 2.6, 3.2 μm are displayed in Fig. 1(b).

The isolated nanorod displays its peak enhancement at 2000 cm^{-1} (5 μm in wavelength). The enhancement spectrum varies with d_y, and shows 'crests' at around the original resonance of 2000 cm^{-1} and along the critical periodicity [5] (or the diffractive coupling condition) of d_c

$= m(\lambda/n)$, where m is an positive integer, λ is the vacuum wavelength, and n is the refractive-index of the substrate. The linewidth is broadened for d_y much smaller than $d_c \sim 3.6$ µm ($\lambda = 5$ µm and $n = 1.4$) and is narrowed with increased field enhancements as d_y approaches d_c. The FWHM of the 'intensity' enhancement (square of the field enhancement) is calculated to be 560 cm^{-1} for the isolated nanorod and changes dramatically with d_y, as 1200, 290, 180 cm^{-1} for $d_y = 1.0$, 2.6, and 3.2 µm, respectively. Correspondingly, the peak value of the field enhancement is 40 for the isolated nanorod and changes with d_y, as 25, 65 and 80 for $d_y = 1.0$, 2.6, and 3.2 µm, respectively.

The observed behavior is understood as follows [12]. The periods d_y's much smaller than the critical period d_c lead to a broadening of the spectral response and a decrease in the near-field intensity, because the dipolar field interactions are rather out of phase. The periods d_y's slightly smaller than d_c lead to a narrowing of the spectral response and an increase in the near-field intensity, because the dipolar field interactions are almost in phase. At the critical condition, its radiative nature leads to a broadening of the spectral response and a drop of the near-field intensity. In this way, periodic arrays generate a collective response resulting in strongly enhanced near-fields compared with an isolated nanoantenna.

Temporal responses of the near-field enhancements are numerically investigated by FDTD simulations. Figure 2 shows the temporal waveforms of the incident electric-field of 100-fs duration, enhanced near-field for the isolated nanorod, and enhanced near-field for the arrays of $d_y = 3.2$ µm. Here the waveforms are normalized to the peak amplitude of the incident electric-field. The peak electric-field is enhanced by 40 times for the isolated nanorod, and 70 times for the arrays of $d_y = 3.2$ µm (close to the collective resonance condition). Such large field enhancement is accompanied by slight elongation of the temporal duration: 120 fs for the isolated nanorod and 140 fs for the arrays of $d_y = 3.2$ µm.

From these results, we can say that the collective-resonance nanorod arrays are beneficial for higher near-field enhancements and therefore higher signal sensitivity, but sacrificing the time resolution and the available bandwidth. In practice, one should choose adequate d_y to balance the magnitude and the bandwidth of the near-field enhancement, according to the specifications required for each experiment. In order to resolve molecular dynamics with high signal sensitivity, one may tune the plasmonic damping to be slightly faster than the molecular dynamics (the typical time scale varies from tens of femtoseconds to tens of picoseconds in condensed phases). In order to elucidate the coupling among different vibrational modes, one may tune the bandwidth so as to cover these vibrational modes.

2.2 Amplification of nonlinear vibrational signals

It has been shown that the linear vibrational signals are amplified with Fano-like lineshapes by nanoantennas resonant to molecular vibrations [5,6]. The Fano-like lineshapes can be explained from the classical coupled oscillator model, where the response of an optically-bright oscillator (nanoantenna) is modulated through the coupling to an optically-dark oscillator (molecular vibration) [16]. The coupled-point-dipole model also reproduces the Fano-like lineshapes [17].

The linear infrared absorption signal A and the third-order nonlinear vibrational signal S can be related to the plasmonic field-enhancement factor L ($= |H(\omega)|$) as [7]

$$A \propto \mu^2 E^2 \big/ 3 \propto L^2, \tag{1}$$

$$S \propto \mu^4 E^4 \big/ 5 \propto L^4, \tag{2}$$

where µ is the transition dipole moment and E is the electric-field. The fourth-power dependence of S on L is understood as follows [7]. Firstly, third-order nonlinear polarization of a molecule driven in the near-field is amplified by a factor of L^3. Secondly, the field radiated by the nonlinear polarization is amplified by forming the image polarization in the nanoparticle/nanoantenna, as is well known for light scattering phenomena [18]. Degree of

this amplification is approximately that of field enhancement L, giving in total an L^4-dependence.
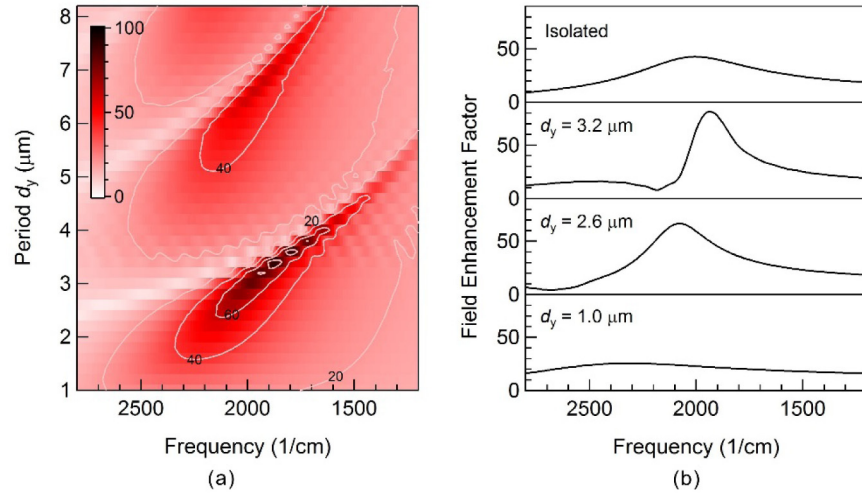

Fig. 1. (a) Local field enhancement factor of gold nanorod arrays for varied d_y. The 'crests' are observed at d_y's slightly smaller than the critical period d_c, which is multiples of the optical wavelength in the substrate. (b) Field enhancement spectra for d_y = 1.0, 2.6, 3.2 μm and infinity (isolated).
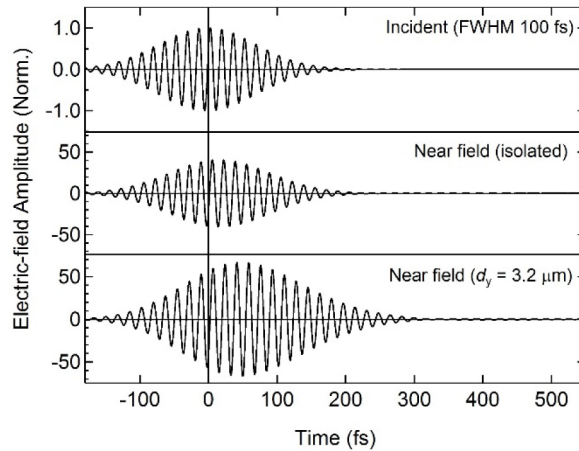

Fig. 2. Temporal waveforms of the incident electric-field of 100-fs duration, enhanced near-fields for the isolated nanorod and for nanorod arrays of d_y = 3.2 μm.

3. Linear extinction spectra of antenna-molecule systems

3.1 Fabrication of nanoantenna arrays

Gold nanorod arrays are fabricated on a CaF_2 substrate by electron-beam lithography and lift-off process. We fabricate two different array patterns, namely, the closely-arranged structure and the (near) collective-resonance structure. In both structures, an elementary nanorod is arranged in 2D arrays of rectangular lattice, where radiative dipolar coupling modifies plasmonic responses but near-field coupling has negligible effects.

Figures 3 (a) and 3(b) show scanning-electron microscope (SEM) images of the closely-arranged structure and the collective-resonance structure. In the former structure, the arrangement period along x-axis (parallel to the longer-axis of the nanorod) and that along y-

axis (parallel to the shorter-axis of the nanorod) are d_x = 2.2 μm and d_y = 1.0 μm, respectively. This d_y is much smaller than d_c ~3.6 μm for λ = 5 μm. In the latter structure, the periods are set to be d_x = 1.9 μm and d_y = 3.3 μm, where d_y is slightly smaller than the critical period d_c, so as to achieve nearly in-phase dipolar couplings and collective excitations at λ = 5 μm. The length, width, and height of the elementary nanorod in the former are 1800 nm, 200 nm, and 30 nm, respectively, and those in the latter are 1450 nm, 200 nm, and 30 nm, respectively. These dimensions are chosen such that the resonance of the collective nanoantenna excitation matches with the molecular vibrational resonance.

3.2 Linear extinction spectra

Far-field normal transmission spectra are measured by FT-IR spectrometer (JASCO FT/IR-4000) with a resolution of 2 cm^{-1} and an averaging number of 30 scans. Thermal light source has a spot diameter of 5 mm at the sample position and therefore ensemble average for a number of nanorods is measured. An IR polarizer is used to measure the transmittance for each polarization direction.

We choose triply-degenerated anti-symmetric CO-stretch vibration (T_{1u} mode) of $W(CO)_6$ dispersed in PMMA as a target mode, where $W(CO)_6$ is a model compound well-studied in nonlinear vibrational spectroscopy [19]. Because the molecules are randomly oriented in PMMA, regardless of the existence of nanorods, and because the near-fields in the vicinity of the nanorod-ends have the same polarization states as the incident linearly-polarized light, the fraction of the excitable molecules among randomly-oriented ensemble is equivalent for two cases of with and without nanorods.

An extinction spectrum for a $W(CO)_6$-dispersed PMMA film of 180-nm thickness, deposited directly on a CaF_2 substrate, is shown in Fig. 4(a) (top panel). The observed absorption peak (FWHM linewidth) is at 1976 cm^{-1} (19 cm^{-1}) for T_{1u} mode of $W(CO)_6$ and at 1731 cm^{-1} (14 cm^{-1}) for CO-stretching mode of PMMA, respectively.

The dotted line in Fig. 4(a) (bottom panel) shows an extinction spectrum for the closely-arranged nanorod arrays. The broad peak due to half-wave dipole antenna resonance is observed at 2250 cm^{-1} with a FWHM linewidth of 970 cm^{-1}. The solid line in the bottom panel is the extinction spectrum for the 180-nm thick $W(CO)_6$: PMMA film deposited on the closely-arranged arrays. Here the extinction spectra are measured for polarization direction parallel to the longer-axes of the nanorods. The frequency for the maximum extinction shifts from 2250 cm^{-1} to 2000 cm^{-1} upon film deposition, due to the change in the surrounding refractive index. The vibrational signal of the guest molecule $W(CO)_6$, as well as that of the host material PMMA, is amplified with Fano-like spectral modifications [5,6].

An extinction spectrum for $W(CO)_6$-dispersed PMMA film of 80-nm thickness, deposited directly on a CaF_2 substrate, is shown in the top panel of Fig. 4(b). The dotted line in Fig. 4(b) (bottom panel) shows an extinction spectrum for the nanorod arrays of (near) collective resonance. The sharp feature (FWHM linewidth of 190 cm^{-1}) clearly indicates the (near) collective resonance where the dipolar field interactions are almost in phase. After deposition of 80-nm-thick sample, peak shift and spectral modifications characteristic to Fano-like resonance occur as shown as a solid line in the bottom panel. Here the vibrational signals are amplified more efficiently than the case of the closely-arranged structure, as will be described in subsection 4.3.
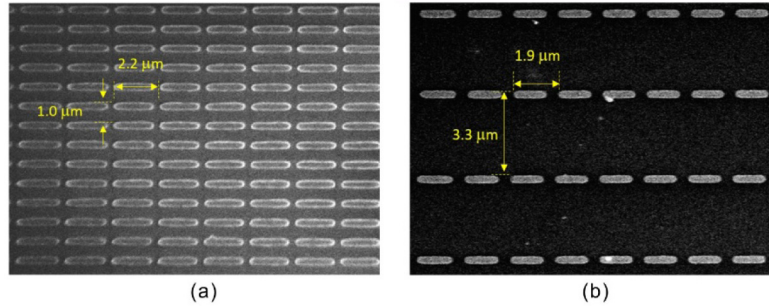
Fig. 3. SEM images of (a) the closely-arranged structure and (b) the collective-resonance structure. The arrangement period along x-axis /y-axis is d_x ~2.2 μm/d_y ~1.0 μm for the former and d_x ~1.9 μm/d_y ~3.3 μm for the latter.
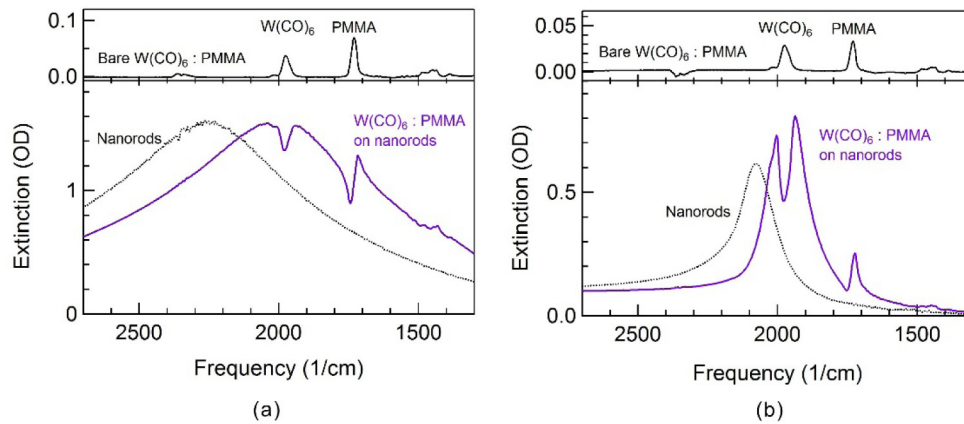

Fig. 4. (a) Extinction spectra for the closely-arranged nanorod arrays on a CaF_2 substrate with and without 180-nm-thick $W(CO)_6$:PMMA film are displayed as a dotted line and a solid line, respectively (the lower panel). The upper panel is for the same film deposited directly on a CaF_2 substrate. (b) Extinction spectra for the nanorod arrays of collective resonance on a CaF_2 substrate with and without the 80-nm-thick $W(CO)_6$:PMMA film are displayed as a dotted line and a solid line, respectively (the lower panel). The upper panel is for the same film deposited directly on a CaF_2 substrate.

4. IR Pump-probe extinction spectroscopy

4.1 Experimental setup

We perform single-color IR pump–probe extinction spectroscopy using the setup described in Ref [20]. A Ti:sapphire regenerative amplifier generates 1 mJ, <100-fs pulses at 1-kHz repetition rate. The subsequent optical parametric amplifier (2-mm thick β-BaB_2O_4, type II) and the difference frequency generator (0.5-mm thick $AgGaS_2$, type II) produce MIR pulses of a few micro-joule energy. A small fraction of the MIR pulses is split off with a wedged BaF_2 window to obtain probe and reference pulses, and the remainder is used for the pump. The pump energy is adjusted with a half-wave plate and a wire-grid polarizer. The linearly polarized pump and probe pulses are focused by means of an off-axis parabolic mirror (an effective focal length of 108.9 mm) and are overlapped in a sample placed at the position where the pump beam diameter is 400 μm. The spectra of the pump and probe pulses are centered at 2000 cm^{-1} with a FWHM bandwidth of 180 cm^{-1}. The time resolution of the pump–probe measurements is about 100 fs.

4.2 Results and discussions

Figure 5 summarizes linear and nonlinear extinction spectra for 5(a)-5(c) the $W(CO)_6$:PMMA film on the closely-arranged nanorod arrays (the sample thickness of 180 nm and the pump energy of 50 nJ), for 5(d)-5(f) the $W(CO)_6$:PMMA film on the collective-resonance nanorod arrays (the sample thickness of 80 nm and the pump energy of 10 nJ), and for 5(g)-5(i) the $W(CO)_6$:PMMA film directly deposited on a CaF_2 substrate (the sample thickness of 180 nm and the pump energy of 890 nJ). Figures 5(a), 5(d), and 5(g) show linear extinction spectra, 5(b), 5(e), and 5(h) show the pump-probe extinction changes at varied delay times and 5(c), 5(f), and 5(i) display the pump-probe extinction changes plotted against the probe frequency and the delay time.

The bare sample film displays typical pump-probe vibrational absorbance changes. Bleaching at the fundamental transition frequency and induced absorption at the red-shifted frequency appear immediately after excitation and decay monotonically, as shown in Figs. 5 (h) and 5(i). The bleaching signal is attributed to population depletion of the $v = 0$ ground state and stimulated emission from the $v = 1$ state (v is the vibrational quantum number). The induced absorption at the red-shifted frequency is attributed to excited-state absorption ($v = 1$–2). The pump-probe extinction changes for the samples on the nanorod arrays shown in Figs. 5 (b), 5(c), 5(e), and 5(f) display similar behaviors as the typical pump-probe absorbance changes, except for their signs. The inversion of the signs is reasonably explained as that molecular vibrational signals are observed through Fano-like resonant interactions with nanoantennas. Then the increased extinction at around the fundamental transition frequency is attributed to the population depletion of the $v = 0$ state and stimulated emission from the $v = 1$ state, whereas the decreased extinction at the red-shifted frequency is attributed to the excited-state absorption of the $v = 1$-2 transition.

The kinetic data for the probe frequencies where positive and negative extinction changes are maximized are summarized in Fig. 6. For the bare sample shown in Fig. 6(c), two decay components with time constants of 8 ps and 70 ps are extracted by the global fitting with a double-exponential function. The faster decay is attributed to anisotropy decay due to intramolecular energy transfer among three degenerate T_{1u} vibrational modes, and the slower decay is attributed to the isotropic population relaxation of the T_{1u} mode (Note that the anisotropy decay time of 3-13 ps and the population relaxation time of 124-160 ps have been measured for $W(CO)_6$ dissolved in alkanes [19]).

The kinetic data at the probe frequencies of 1992 and 1958 cm^{-1} for the sample on the closely-arranged nanorod arrays are shown in Fig. 6(a). The global fitting analyses extract two time constants of 11 ps and 58 ps for exponential decays, and an additional time constant of 6 ps for an asymptotic growth. Referring to the dynamics of the bare sample, the 11-ps component and the 58-ps component are attributed to the intramolecular energy transfer and the population relaxation, respectively. The asymptotic growth with a time constant of 6 ps would be attributed to the thermalized response of the gold nanorods [21]. Global fitting analyses on the kinetic data at 1990 and 1951 cm^{-1} for the sample on the collective-resonance arrays extract two time constants of 3 ps (anisotropy decay) and 61 ps (population relaxation) for exponential decays, and a time constant of 6 ps (the thermalized response of the gold nanorods) for an asymptotic growth. In this way, almost identical population relaxation times of 60-70 ps are found for the samples with and without nanorods, whereas the signal enhancements are substantial, as described in the following section.
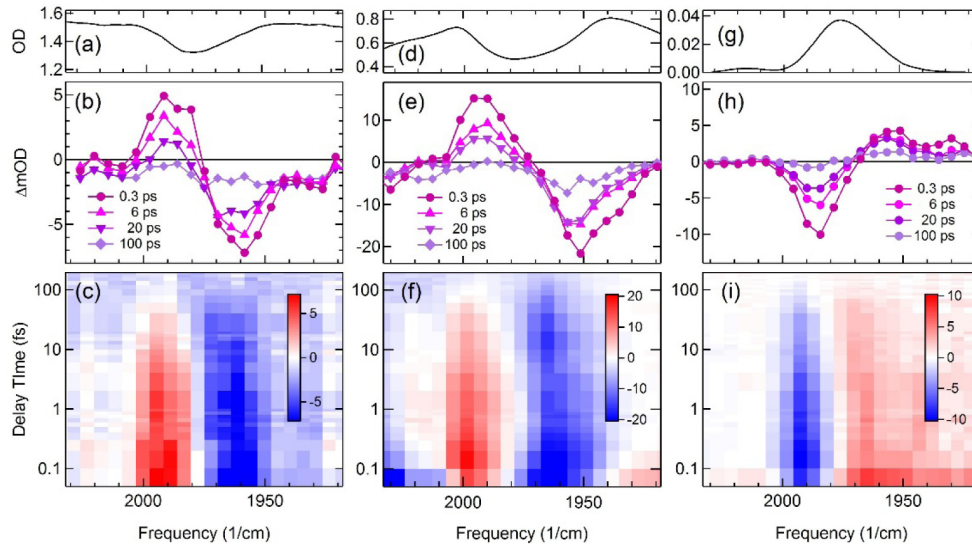
Fig. 5. Linear and nonlinear extinction spectra for (a-c) the $W(CO)_6$:PMMA film on the closely-arranged nanorod arrays (the sample thickness of 180 nm and the pump energy of 50 nJ), for (d-f) the $W(CO)_6$:PMMA film on the collective-resonance nanorod arrays (the sample thickness of 80 nm and the pump energy of 10 nJ), and for (g-i) the $W(CO)_6$:PMMA film directly deposited on a CaF_2 substrate (the sample thickness of 180 nm and the pump energy of 890 nJ). (a,d,g) Linear extinction spectra, (b,e,h) pump-probe extinction changes at varied delay times, (c,f,i) pump-probe extinction changes plotted against the probe frequency and the delay time. The scale-bars show the extinction changes in mOD.
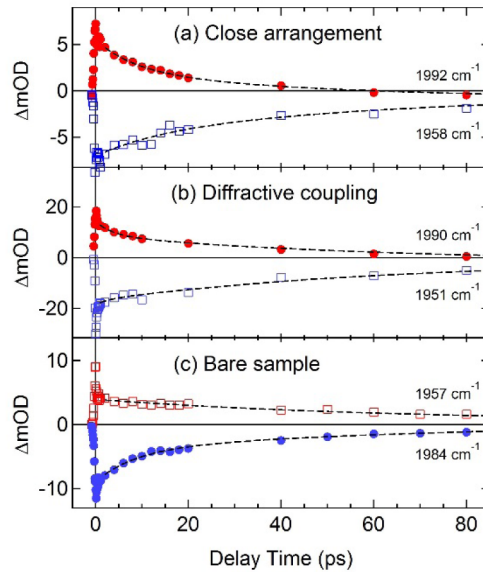

Fig. 6. The kinetic data for the probe frequencies of $v = 0 \rightarrow 1$ (circles) and $1 \rightarrow 0$ (squares) transitions and the corresponding fitted curves (dashed lines) are shown for (a) the sample on closely-arranged nanorod arrays, for (b) the sample on collective-resonance nanorod arrays, and (c) the sample directly deposited on a CaF_2 substrate.

4.3 Signal enhancement factors

One can find that the extinction changes are comparable among the three measurements shown in Figs. 5 (b), 5(e), and 5(h), in spite of different pump energy of 50 nJ, 10 nJ, and 890 nJ, respectively. It indicates that the nonlinear signal is substantially amplified by the nanorod arrays. The impact of nanorods is also clearly found in Fig. 7, the pump-probe extinction changes at 0 ps for different pump polarizations (parallel and perpendicular to the nanorods). Here the sample is deposited on the closely-arranged arrays, the pump energy is kept constant, and the probe polarization is kept parallel to the nanorods in both cases. Extinction changes are clearly observed only for the pump polarization parallel to the nanorods.
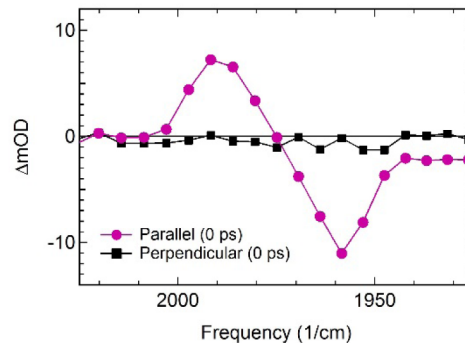

Fig. 7. The pump-probe extinction changes at 0 ps for the sample on the closely-arranged structure, when the pump polarization is parallel or perpendicular to the nanorods. The probe polarization is kept parallel to the nanorods in both cases.

Here we estimate and discuss the linear and nonlinear signal enhancement factors. As presented in section 3, we performed experiments for two series of the samples. Series I is for the sample with/without the closely-arranged nanorod arrays (the sample thickness of 180 nm). Series II is for the sample with/without the collective-resonance nanorod arrays (the sample thickness of 80 nm).

By analyzing the extinction spectra shown in Figs. 4(a) and 4(b), we find that the linear extinction signal of $W(CO)_6$ is amplified by 5.0 times by the coupling with closely-arranged nanorod arrays and by 16 times by the coupling with collective-resonance nanorod arrays. By assuming that the signals come only from the hot spots near the extremities of the nanorods, the local signal enhancement factor is estimated to be 4.1×10^3 and 1.7×10^4 for the closely-arranged and the collective-resonance structures, respectively. Here the local signal enhancement factor is estimated as the above-mentioned amplification factor (5.0 and 16) divided by the fractional hot-spot volume, calculated as follows. Since the width, height and decay length of the near-field, estimated from FDTD simulations are 200 nm, 30 nm, and 40 nm, respectively, the hot-spot volume per nanorod is calculated to be 480,000 nm^3. For measurements without antennas, on the other hand, signals are generated from all the volume of the sample film through which the beam propagates. Here the fractional hot-spot volume can be calculated as the hot-spot volume per nanorod divided by the unit-cell volume (2200 × 1000 × 180 nm^3 and 1900 × 3300 × 80 nm^3) to be 1.2×10^{-3} and 0.96×10^{-3} for the closely-arranged and the collective-resonance structures, respectively. The field enhancement factor is estimated as the square root of the local signal enhancement factor to be 64 and 130 for the closely-arranged and the collective-resonance structures, respectively. The fact that the collective-resonance condition gives higher signal enhancement is consistent with our FDTD simulations shown in Fig. 1(a,b) and with previous studies [6, 12–15].

Table 1 summarizes the parameters of nonlinear measurements: pump energy, extinction change (peak-valley difference at 0.3 ps), signal per unit pump energy (or 'averaged' signal

enhancement factor estimated for 80-nm-thick sample), fractional hot-spot volume, and signal per unit pump energy and unit volume (or 'local' signal enhancement factor).

The 'averaged' nonlinear signal enhancement factor is estimated as extinction change divided by pump energy, and then normalized by its value for the bare sample. This is understood as the signal enhancement, spatially-averaged over the sample plane within the beam spot. Here we note that the spatially-averaged enhancement factor is affected by sample thickness, because local signal enhancement strongly depends on the distance from the nanoantenna surface [12, 22]. In order to have reasonable comparison between the two array structures, we assume common sample thickness of 80 nm. In fact, we adopt extinction change of 6.2 mOD for the bare sample of Series I (calculated from 14 mOD for 180-nm-thick bare sample). Extinction change of the sample with closely-arranged nanorod arrays is assumed to be same for different thicknesses of 80 and 180 nm, because the signal enhancement diminishes beyond 100 nm [22]. Now the averaged enhancement factor is estimated to be 34 and 850 for the closely-arranged and the collective-resonance structures, respectively. The signal enhancement is much larger for the latter structure that has smaller hot-spot volume, which fact clearly shows the impact of the dipolar coupling.

The local enhancement factor of the nonlinear signal is estimated by assuming that signals come only from the hot spots near the extremities of the nanorods, similar to the case of the linear signals. Here we note that the assumed hot-spot volume is different for the linear and the nonlinear measurements. In the linear (nonlinear) measurement, the decay length of the hot-spot is defined as the length at which the near-field intensity decays to $1/e^2$ ($1/e$) of its maximum, and is estimated to be 40 nm (20 nm). We exploit these definitions, considering that the linear (nonlinear) signal is proportional to the square (the fourth-power) of optical field as shown in Eqs. (1,2). The local nonlinear signal enhancement factor, calculated as the signal amplitude per unit pump energy and unit volume, is estimated as 2.5×10^4 and 1.8×10^6 for the closely-arranged and the collective-resonance structures, respectively. Correspondingly, the near-field enhancement factor L is estimated as 13 and 37 from Eq. (2).

In this way, the trend that the collective-resonance brings about larger enhancements in the linear and the nonlinear signals is clearly demonstrated. Though the field enhancement factors extracted from the linear measurements (64 and 130) and those extracted from the nonlinear measurements (13 and 37) are somewhat different from those predicted by FDTD simulations (25 and 80), shown in Figs. 1(a) and 1(b), it is consistently observed that the collective-resonance structure gives 2-3 times higher field enhancement than the closely-arranged one does. Possible reasons for smaller field enhancements extracted from nonlinear measurements include saturable response of the nanoantenna array and degraded plasmon resonance in pump−probe measurements (the polarization directions of the pump and probe pulses may be slightly deviated from nanoantenna axes, because of the technical limitations).

Table 1. Parameters of the pump-probe experiments.

	Series I		Series II	
Antenna arrangement	w/o antennas	Closely arranged	w/o antennas	Collective resonance
Pump energy (nJ)	890	50	1490	10
Nonlinear signal (Extinction change at 0.3 ps, mOD)	14	12	6.5	37
Signal per unit pump energy for 80-nm thickness (norm.)	1	34	1	850
Fractional hot-spot volume	1	0.61×10^{-3}	1	0.48×10^{-3}
Signal per unit pump energy and unit volume (norm.)	1	2.5×10^4	1	1.8×10^6

5. Summary

We successfully demonstrate surface-enhanced nonlinear vibrational spectroscopy using periodic gold nanoantenna arrays. Especially, we show that the dipolar coupling among nanoantennas has striking impact on near-field enhancements and nonlinear vibrational signal enhancements. The IR pump-probe spectroscopy measurements on a $W(CO)_6$:PMMA film elucidate that the condition near the collective-resonance achieves effective signal enhancement of 850 times and local signal enhancement of 1.8×10^6 times, reducing required pump energy from micro-joule to nano-joule level. The observed vibrational dynamics is almost identical regardless of the signal enhancements by nanoantenna arrays.

Such substantial signal enhancement should be beneficial in increasing the signal strength with conventional MIR pulsed light sources of micro-joule level, and therefore useful for characterizing structure and dynamics of minute-volume molecules and for detecting vibrational modes with smaller transition moments. The signal enhancement, together with surface sensitivity, is also useful for investigating monolayers and interfaces, which are important in the field of structural biology, photo-catalysis, and organic electronics. The substantial signal enhancement is also beneficial in obtaining nonlinear signals with a reduced excitation pulse energy. In this respect, the demonstrated scheme paves the way to nonlinear vibrational spectroscopy measurements with compact light sources of oscillator-level. Such simplification of the whole system is a critical key for nonlinear vibrational spectroscopy to become widely-used. The oscillator-level pulsed sources generate pulses at higher repetition rates, which is advantageous for shorter data acquisition time. Further engineering in the metal nanostructure as well as the beam geometry [23] is promising for even higher sensitivity and new functionality.